

Sampling error mitigation through spectrum smoothing in ensemble data assimilation

Bosu Choi* and Yoonsang Lee†

Department of Mathematics, Dartmouth College

April 2, 2024

Abstract

In data assimilation, an ensemble provides a nonintrusive way to evolve a probability density described by a nonlinear prediction model. Although a large ensemble size is required for statistical accuracy, the ensemble size is typically limited to a small number due to the computational cost of running the prediction model, which leads to a sampling error. Several methods, such as localization, exist to mitigate the sampling error, often requiring problem-dependent fine-tuning and design. This work introduces another sampling error mitigation method using a smoothness constraint in the Fourier space. In particular, this work smoothes out the spectrum of the system to increase the stability and accuracy even under a small ensemble size. The efficacy of the new idea is validated through a suite of stringent test problems, including Lorenz 96 and Kuramoto-Sivashinsky turbulence models.

Keywords— data assimilation, sampling error mitigation, ensemble Kalman filter, spectrum smoothing

1 Introduction

Data assimilation seeks to effectively combine time-ordered observations with models to predict accurate state estimates of dynamical systems. It was initially developed for weather prediction and has been widely used in many areas, such as geoscience, robotics, and oceanography. Its algorithmic development has progressed in multiple research areas, and Bayesian formulation sets a mathematical foundation of data assimilation [14]. Among data assimilation approaches, including interpolation, smoothing, and filtering, this paper focuses on filtering problems. It generally consists of two steps: i) prediction to evolve state estimates using prediction models and ii) analysis to update

*bo.su.choi@dartmouth.edu

†yoonsang.lee@dartmouth.edu

the state estimates by combining models and observations. If both model and observation operator are linear with additive and state-independent model and observational errors, Kalman filter [12] is the optimal data assimilation method. However, many problems of interest in various areas are nonlinear, which encourages the development of diverse filtering methods, including variational methods [13], particle filter [7], extended Kalman filter [11], ensemble Kalman filter [6]. More recently, nonlinear ensemble filtering in [17] generalizing the ensemble Kalman filter (EnKF) reduces the intrinsic bias of EnKF at a marginal increase in computational cost by using transport maps.

If the dynamical system is nonlinear with non-Gaussian assumption, Kalman filter does not provide the optimal approach. Alternatively, the ensemble Kalman filter uses sample called “ensemble” to better approximate non-Gaussian distribution by evolving it by a nonlinear evolution operator in the prediction step and updating them by combining sequential observations and models. EnKF is interpreted as a Monte Carlo implementation of the sequential Bayesian method, which is related to the particle filter, but the particle filter is suitable for lower dimensional problems. To make data assimilation effective for high dimensional nonlinear problems, ensemble square root filter (ESRF) [18] and ensemble transform Kalman filter (ETKF) [19] use linear transformations to update a prior ensemble to a posterior ensemble in the analysis step. Though transform matrices update an ensemble conveniently, covariance matrices crucial for accurate analysis can be poorly estimated due to sampling errors and spurious correlation.

Localization [8] together with inflation [1] is essential to reduce sampling errors in ensemble methods. Their performances are sensitive to the ensemble size, which is the size of sample from probability distributions. Therefore, a larger ensemble size is required depending on the dimensions. However, when it is computationally expensive to evolve an ensemble by a nonlinear prediction model, the ensemble size cannot be increased as it is desired for accurate data assimilation at a decent speed. Instead, localization reduces the sampling errors due to the small ensemble size and remedies the issues from the low-rank approximation. It is often to determine the localization based on the displacement, which makes the localization symmetric, but for more sophisticated and data-driven design of localization using convolutional neural networks is suggested in [20]. On the other hand, inflation mitigates model and sampling errors by maintaining the ensemble variance large. Inflating the covariance is also interpreted as adjusting the regularization parameter and balancing the weights for new observations and priors. Localization and inflation reduce the effect of sampling errors in ensemble methods to some extent. However, their influence is still limited, especially when observations are sparse due to the limitation of measurement resources, and the ensemble size is small due to the computational cost. The authors of this work consider target states’ inherent smooth constraint to mitigate the sampling error more strongly and to make ensemble methods more stable in disadvantageous circumstances regarding the ensemble number and observation characteristics. Therefore, the prior ensemble is updated in a way that it reflects the desired probability distribution better without increasing its size.

Appropriate covariance estimation is a key ingredient for successful data assimilation, which is achieved by mitigating the sampling errors. Chaotic systems show disorder and irregular trajectories in the physical domain, which makes it more difficult to predict the future state. However, under certain assumptions on random processes depicting the chaotic behavior statistically, global characteristics of the chaotic solutions can be captured considering a spectrum of ensemble in Fourier domain. Khinchin Theorem also supports the usefulness of the spectrum in describing the important solution feature: correlation between state variables. It implies that the correlation and energy spectrum are one-to-one Fourier pairs for stationary random processes, i.e., the energy spectrum determines the correlation uniquely. This motivated authors to update ensemble to mitigate

the sampling errors using the spectrum of ensemble so that the updated ensemble approximate the energy spectrum of the target state more precisely. If we increase the ensemble size large enough, its spectrum is expected to be close to the target state's spectrum, which is smooth by the turbulence theory. Therefore, the authors make the updated ensemble to have a smoother spectrum than before, and accordingly, the ensemble better reflects the true probability distribution by sampling error mitigation and accordingly alleviate the spurious correlation.

The rest of this paper is organized as follows. In Section 2, our problem setting for the data assimilation focusing on ETKF and the classical sampling error mitigation methods are reviewed. Then, in Section 3, we discuss our method for mitigating the sampling error using the smooth constraint and its motivation using turbulence theory. In Section 4, our method and the classic data assimilation are compared numerically when applied to predict the state of chaotic dynamical systems, including the Lorenz 96 model and Kuramoto-Sivashinsky equation. A summary of our work and discussion for the future directions are provided in Section 5.

2 Data assimilation

We introduce the notation used throughout this article. Furthermore, we introduce our problem setting in Section 2.1 and review the Kalman filter, focusing on the ensemble transform Kalman filter (ETKF) in Section 2.2. In Section 2.3, we introduce classic techniques to improve the performance of ensemble methods by reducing errors from sampling, model, and other possible sources and estimating a more appropriate covariance matrix for data assimilation.

2.1 Problem setting

We consider a dynamical system with the state solution $\mathbf{v}(t) \in \mathbb{R}^N$ and time $t \in [0, T]$. We discretize the time as $t_j = j\Delta t$ for $j = 0, 1, \dots, J$ and $\Delta t = \frac{T}{J}$ with a terminal time step $J \in \mathbb{N}$. We denote the discrete evolution (or prediction) operator as $\Psi : \mathbb{R}^N \rightarrow \mathbb{R}^N$, and the observation as \mathbf{y}_j with the observation operator $h : \mathbb{R}^N \rightarrow \mathbb{R}^M$. Accordingly, the solution trajectory and the observation are modeled as follows:

$$\mathbf{v}_{j+1} = \Psi(\mathbf{v}_j) \tag{1}$$

$$\mathbf{y}_{j+1} = h(\mathbf{v}_{j+1}) + \boldsymbol{\gamma}_{j+1}, \tag{2}$$

where $j = 0, 1, \dots, J-1$, and the observation noise, $\boldsymbol{\gamma}_{j+1}$, follows the Gaussian distribution $\mathcal{N}(\mathbf{0}, \Gamma)$. In this work, we are interested in assimilating the dynamical model and observations, particularly in filtering problems for predicting future states by sequentially updating the posterior distribution of the state solution from its prior distribution and new observations using Bayes' formula.

2.2 Ensemble Transform Kalman Filter (ETKF)

Kalman filter assumes that both Ψ and h are linear, i.e.,

$$\Psi(\mathbf{v}_j) = M\mathbf{v}_j, \quad h(\mathbf{v}_j) = H\mathbf{v}_j, \tag{3}$$

and the prior distribution is Gaussian, which implies that the posterior distribution is Gaussian as well, and accordingly, the updates of mean and covariance fully characterize the evolution of distribution. Although the analysis of the Kalman filter is based on the linearity assumption,

variants of the Kalman filter are successfully applicable to nonlinear models. One of them is the ensemble Kalman filter (EnKF), which uses an ensemble to estimate the covariance matrix for the Kalman update. If the ensemble size, K , is small, then the covariance estimation degrades due to the sampling error and spurious correlation. Therefore, it is beneficial to choose a sufficiently large ensemble size depending on the model and the dimensions, N , of state variables. However, increasing the ensemble size is less preferred when numerical solvers for (1) have large computational complexity. In order to reduce errors due to the small ensemble size and other sources and to improve the performance of the data assimilation, various methods have been developed, including localization, inflation, and sampling error correction, which are reviewed in Section 2.3.

Ensemble transform Kalman filter (ETKF) updates the covariance by linearly transforming the ensemble by multiplying a transform matrix. Generally, the Kalman filter has two steps: prediction and analysis. Here, we describe how these steps are processed in EnKF and ETKF. In the prediction step, each ensemble member, $\mathbf{v}_j^{(k)}$, is propagated by the evolution operator to evolve the mean, $\hat{\mathbf{m}}_{j+1}$, and covariance, \hat{C}_{j+1} , of the state solution as follows:

$$\hat{\mathbf{v}}_{j+1}^{(k)} = \Psi(\mathbf{v}_j^{(k)}), \quad k = 1, \dots, K \quad (4)$$

$$\hat{\mathbf{m}}_{j+1} = \frac{1}{K} \sum_{k=1}^K \hat{\mathbf{v}}_{j+1}^{(k)} \quad (5)$$

$$\hat{C}_{j+1} = \frac{1}{K-1} \sum_{k=1}^K (\hat{\mathbf{v}}_{j+1}^{(k)} - \hat{\mathbf{m}}_{j+1})(\hat{\mathbf{v}}_{j+1}^{(k)} - \hat{\mathbf{m}}_{j+1})^T. \quad (6)$$

The prediction step is performed for each time step $j = 0, 1, \dots, J-1$. On the other hand, the analysis step is carried out only at the time step when a new observation comes in. The ensemble is updated based on the posterior distribution by combining the prior and observation, and consequently, the posterior mean and covariance are obtained as follows:

$$K_{j+1} = \hat{C}_{j+1} H^T (H \hat{C}_{j+1} H^T + \Gamma) \quad (7)$$

$$\mathbf{m}_{j+1} = \hat{\mathbf{m}}_{j+1} + K_{j+1} (\mathbf{y}_{j+1} - H \hat{\mathbf{m}}_{j+1}) \quad (8)$$

$$\mathbf{v}_{j+1}^{(k)} = \mathbf{m}_{j+1} + \boldsymbol{\zeta}_{j+1}^{(k)}, \quad (9)$$

where K_{j+1} is the Kalman gain. Here, $\boldsymbol{\zeta}_{j+1}^{(k)}$ are designed to have posterior covariance $C_{j+1} = (I - K_{j+1} H) \hat{C}_{j+1}$ in EnKF. On the other hand, ETKF updates the covariance by multiplying a transform matrix $T_{j+1}^{1/2}$ to the matrix, \hat{X}_{j+1} , whose columns are the centered ensemble members as the following:

$$\hat{X}_{j+1} = \frac{1}{\sqrt{K-1}} \left[\hat{\mathbf{v}}_{j+1}^{(1)} - \hat{\mathbf{m}}_{j+1}, \dots, \hat{\mathbf{v}}_{j+1}^{(K)} - \hat{\mathbf{m}}_{j+1} \right] \quad (10)$$

$$T_{j+1} = [I + (H \hat{X}_{j+1})^T \Gamma^{-1} (H \hat{X}_{j+1})]^{-1} \quad (11)$$

$$X_{j+1} = \hat{X}_{j+1} T_{j+1}^{1/2}. \quad (12)$$

Then, the prior and posterior covariance matrices are obtained as intended by using the transform matrix $T_{j+1}^{1/2}$, i.e.,

$$\hat{C}_{j+1} = \hat{X}_{j+1} \hat{X}_{j+1}^T, \text{ and } C_{j+1} = X_{j+1} X_{j+1}^T = (I - K_{j+1} H) \hat{C}_{j+1}. \quad (13)$$

The posterior mean, \mathbf{m}_{j+1} , is equivalent to the mean of the posterior ensemble, $\mathbf{v}_{j+1}^{(k)}$, and also to the solution of regularized optimization in the following:

$$\arg \min_{\mathbf{v}} \frac{1}{2} \|\mathbf{y}_{j+1} - H\mathbf{v}\|_{\Gamma}^2 + \frac{1}{2} \|\mathbf{v} - \hat{\mathbf{m}}_{j+1}\|_{\hat{C}_{j+1}}^2, \quad (14)$$

where $\|\mathbf{v}\|_C^2 := \mathbf{v}^T C^{-1} \mathbf{v}$ represents the ℓ_2 norm of a vector, \mathbf{v} , weighted by a matrix, C .

2.3 Classic methods for sampling error mitigation

Ensemble-based data assimilation approaches effectively extend the Kalman filter to solve nonlinear problems. However, their performances fluctuate depending on the ensemble size and other factors since the estimation of statistics, including the mean and covariance, deteriorates if the ensemble number is too small to represent the target probability distribution well. When it is required to keep the ensemble size small due to the computational limit, there are various techniques to reduce the errors from sampling or covariance estimation.

Inflation increases the ensemble spread to prevent the variance of distribution from degenerating. It allows the ensemble to have descent variations to explore the solutions. Among many approaches, a simple but frequently used approach to inflating the variance is multiplying a constant inflation factor, $\rho \geq 1$, to the entire covariance matrix. In terms of regularized optimizations, inflation reduces the size of the regularization term, the second term in (14), so that new observations are considered more significantly to update the posterior. On the other hand, localization alleviates the spurious correlation due to the insufficient sample based on the physical distance. It presumes that the correlation between state elements decays if the locations of these elements are far apart. Moreover, it resolves the problem of rank deficiency due to the small ensemble number. From 13, sample covariances are observed to have the rank of, at most, the ensemble size. Localization reduces sampling errors and remedies other issues, making it necessary for ensemble methods even though the ensemble size is large. To demonstrate this, we tested with the ensemble size to 1000 for 40-dimensional Lorenz 96 model and implemented ETKF to solve it. Since the ensemble size is large enough, applying localization would not have made much difference if it were true that localization is necessary only for reducing the sampling error. When applying the localization and inflation, however, the RMSE error of ETKF is decreased by about 10% compared to the ETKF without applying these two methods, which implies that the effect of localization is not limited to the sampling error reduction.

Among various methods for covariance localization, Gaspari-Cohn (GC) function [16] is widely used due to its effectiveness. GC function looks like a Gaussian function, but the support is compact. The resulting localization is symmetric since it determines the localization factor based on the displacement. To explain, GC function, g_c , with a halfwidth, c , is used to determine the localization matrix, L_c , so that the element at i th row and j column is set to $g_c(|i - j|)$. Inflation and localization modify the covariance matrix as follows:

$$\hat{C}_{j+1} \leftarrow \rho L_c \odot \hat{C}_{j+1}, \quad (15)$$

where \odot represents a Hadamard product.

Inflation and localization are essential tools for ensemble-based data assimilation. However, the inflation factor ρ and GC function's halfwidth c are tuning parameters. The performance of ETKF is sensitive to these parameters, and the tuning process can be computationally expensive for complex

models. Therefore, [2] suggests an algorithm to produce localizations based on the ensemble size and ensemble correlation, which results in the sampling error correction. This algorithm performs offline Monte-Carlo simulation to make a lookup table to choose localization depending on the ensemble number and ensemble sample correlation, which is considered to auto-tune the localization. In this work, localization is defined as a factor that determines the increments to the ensemble to correct the sampling errors. This approach is useful, especially for applications where GC localization is suboptimal.

3 Sampling error mitigation based on smoothness constraint

Classic covariance localization often modifies the correlation based on the physical distance, and Anderson [2] adjusts the ensemble based on the sensitivity of each state variable in the physical domain to the observation to correct the sampling error. Instead, the authors in this work pay attention to the characteristics of state variables in the Fourier domain, which helps extract the states' global features. Dynamics, which is chaotic but is a stationary random process, has smooth characteristics in its energy spectrum, which is well studied in Kolmogorov's theory. Moreover, Khinchin's Theorem implies that the autocorrelation and power spectral density are a Fourier pair, i.e., have one-to-one correspondence. These theories motivated the authors to update the ensemble using the smooth feature in the Fourier domain to mitigate the sampling error and improve the correlation estimation accordingly.

3.1 Random field and spectrum

Kolmogorov theory provides a statistical description of turbulence [5]. Statistical approaches assume that point separations within certain scale sizes exhibit the important characteristics of statistical homogeneity and isotropy. In general, statistical homogeneity of the random velocity field implies that the mean value of the field is constant and that correlations between random fluctuations in the field from point to point are independent of the chosen observation points, depending only on their vector separation. Moreover, if the random fluctuations are also statistically isotropic, then point-to-point correlations depend only on the magnitude of the vector separation between observation points.

Let $u(\mathbf{x})$ be a random flow field. Under the assumption of periodicity, we write

$$u(\mathbf{x}) = \sum c_{\mathbf{k}} e^{i\mathbf{k} \cdot \mathbf{x}}, \quad (16)$$

and define the spectral distribution, F , of u as:

$$F(\mathbf{k}) = \sum_{|\mathbf{k}| < k} \langle |c_{\mathbf{k}}|^2 \rangle := \int_{\Omega} |c_{\mathbf{k}}|^2 dP, \quad (17)$$

where (Ω, \mathcal{B}, P) is a probability space and $|\cdot|$ is a Euclidean distance. Under the assumption that F is differentiable, we obtain

$$dF(\mathbf{k}) = \Phi(\mathbf{k}) d\mathbf{k}, \quad (18)$$

where Φ is the spectral density of u . Finally, we define the energy spectrum, $E(k)$, of u as the following:

$$E(k) = \frac{1}{2} \int_{|\mathbf{k}|=k} \Phi(\mathbf{k}) d\mathbf{k}. \quad (19)$$

According to Kolmogorov law, the energy spectrum, $E(k)$, of homogeneous flow follows:

$$E(k) = C\epsilon^{2/3}k^{-5/3}, \quad (20)$$

where C is a dimensionless constant, and $\epsilon = \frac{d}{dt}\langle u^2 \rangle$. Kolmogorov law indicates that the energy spectrum of a random flow field is smooth with a certain decay rate.

Wiener–Khinchin–Einstein theorem or the Khinchin–Kolmogorov theorem, states that the autocorrelation function of a stationary stochastic process has a spectral decomposition given by the power spectral density of the process [3]. The correlation function of $u(\mathbf{x})$ is

$$R(\mathbf{x}_1, \mathbf{x}_2) = \langle (u(\mathbf{x}_1) - m(\mathbf{x}_1))(u(\mathbf{x}_2) - m(\mathbf{x}_2)) \rangle \quad (21)$$

where $m(\mathbf{x})$ is a mean of $u(\mathbf{x})$.

Theorem 1 (Khinchin Theorem). *For a function $R(\mathbf{x})$ to be the correlation function of a field which has translation invariant means and correlation functions and also satisfies the condition*

$$\langle |u(\mathbf{x} + \mathbf{h}) - u(\mathbf{x})|^2 \rangle \rightarrow 0 \text{ as } \|\mathbf{h}\| \rightarrow 0 \quad (22)$$

where $\|\cdot\|$ is a vector norm, it is necessary and sufficient that it has a representation of the form

$$R(\mathbf{r}) := \langle (u(\mathbf{x}) - m(\mathbf{x}))(u(\mathbf{x} + \mathbf{r}) - m(\mathbf{x} + \mathbf{r})) \rangle = \int \exp(i\mathbf{k} \cdot \mathbf{r}) dF(\mathbf{k}). \quad (23)$$

Khinchin Theorem implies that given $F(\mathbf{k})$ (or $\Phi(\mathbf{k})$), $R(\mathbf{x})$ can be constructed with the help of Fourier integrals, i.e., the correlation of state variables in the physical domain has a one-to-one correspondence with the spectral density function.

3.2 Sampling error mitigation

Inspired by the smooth characteristics of the energy spectrum, we adjust ensemble members so that their mean spectrum becomes closer to the true energy spectrum. To obtain a smoothed spectrum that the ensemble is adjusted to fit into, we take a convolution of the ensemble mean spectrum, ϕ , with a smoothing kernel, κ_σ , as follows:

$$(\phi * \kappa_\sigma)(\omega) = \int \phi(\omega - \tau) \kappa_\sigma(\tau) d\tau. \quad (24)$$

Multiplicative rescaling factor α is determined so that the updated ensemble's mean spectrum is close to the smoothed spectrum. Specifically, we update the prior ensemble $\hat{\mathbf{v}}_{j+1}^{(k)} = \hat{\mathbf{m}}_{j+1} + \hat{\mathbf{x}}_{j+1}^{(k)}$, where $\hat{\mathbf{m}}_{j+1}$ is the mean of ensemble, $\frac{1}{N} \sum_{k=1}^K \hat{\mathbf{v}}_{j+1}^{(k)}$. The multiplicative rescaling factor $\alpha(\omega)$ is chosen so that it satisfies the second equality in the following:

$$S_\sigma \left(\frac{1}{N} \sum_{k=1}^K |\mathcal{F}(\hat{\mathbf{v}}_{j+1}^{(k)})|^2 \right) := \begin{cases} \left(\frac{1}{N} \sum_{k=1}^K |\mathcal{F}(\hat{\mathbf{v}}_{j+1}^{(k)})|^2 \right) * \kappa_\sigma \\ \text{if } \left(\frac{1}{N} \sum_{k=1}^K |\mathcal{F}(\hat{\mathbf{v}}_{j+1}^{(k)})|^2 \right) * \kappa_\sigma \geq |\mathcal{F}(\hat{\mathbf{m}}_{j+1})|^2 \\ |\mathcal{F}(\hat{\mathbf{m}}_{j+1})|^2 \text{ otherwise} \end{cases} \quad (25)$$

$$= \frac{1}{N} \sum_{k=1}^K |\mathcal{F}(\hat{\mathbf{m}}_{j+1}) + \alpha \mathcal{F}(\hat{\mathbf{x}}_{j+1}^{(k)})|^2, \quad (26)$$

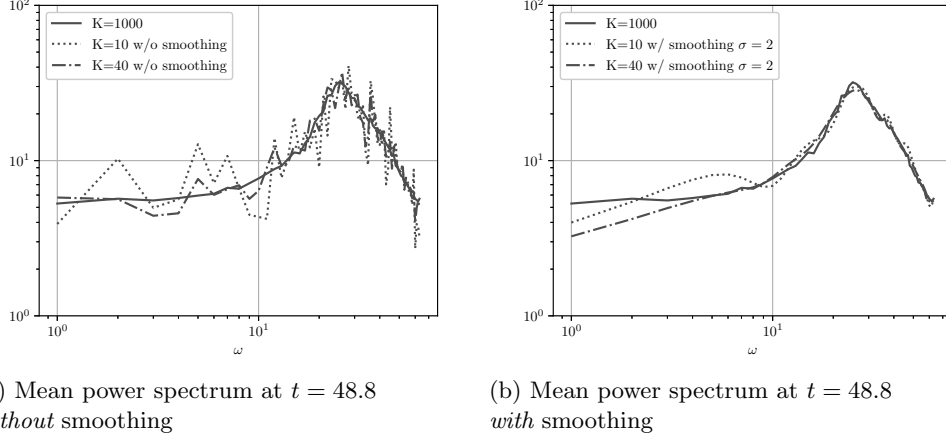


Figure 1: Lorenz 96 sample mean power comparison while varying the sample size: (a) smoothing is *not* applied and (b) smoothing is applied

where $S_\sigma(\cdot)$ is a smoothing operator with a kernel width scaling factor σ and \mathcal{F} is the discrete Fourier transform. The smoothing operator $S_\sigma(\cdot)$ is defined as in (25) to make the rescaling factor α to be a real function. Otherwise, (29) below cannot be well-defined. Using the fact that the sum of deviations, $\hat{\mathbf{x}}_{j+1}^{(k)}$, from the ensemble mean is 0, i.e., $\sum_{k=1}^K \mathcal{F}(\hat{\mathbf{x}}_{j+1}^{(k)}) = 0$, α is determined by simplifying (26) as follows:

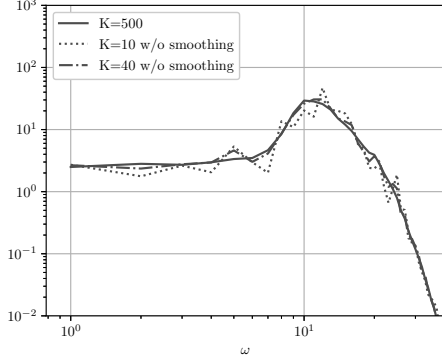
$$S_\sigma \left(\frac{1}{N} \sum_{k=1}^K |\mathcal{F}(\hat{\mathbf{v}}_{j+1}^{(k)})|^2 \right) = |\mathcal{F}(\hat{\mathbf{m}}_{j+1})|^2 + \frac{\alpha^2}{N} \sum_{k=1}^K |\mathcal{F}(\hat{\mathbf{x}}_{j+1}^{(k)})|^2, \quad (27)$$

$$\alpha^2 = \frac{S_\sigma \left(\frac{1}{N} \sum_{k=1}^K |\mathcal{F}(\hat{\mathbf{v}}_{j+1}^{(k)})|^2 \right) - |\mathcal{F}(\hat{\mathbf{m}}_{j+1})|^2}{\frac{1}{N} \sum_{k=1}^K |\mathcal{F}(\hat{\mathbf{x}}_{j+1}^{(k)})|^2} \quad (28)$$

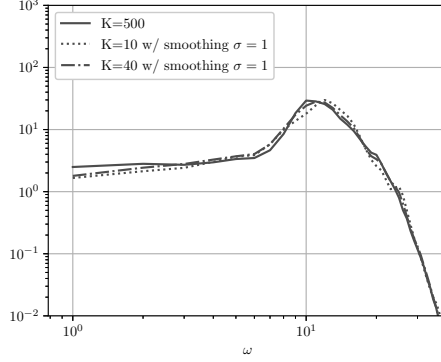
$$\alpha = \sqrt{\frac{S_\sigma \left(\frac{1}{N} \sum_{k=1}^K |\mathcal{F}(\hat{\mathbf{v}}_{j+1}^{(k)})|^2 \right) - |\mathcal{F}(\hat{\mathbf{m}}_{j+1})|^2}{\frac{1}{N} \sum_{k=1}^K |\mathcal{F}(\hat{\mathbf{x}}_{j+1}^{(k)})|^2}}. \quad (29)$$

Here, we choose the nonnegative sign for determining α consistently in order to not switch the phase, and the smoothing operator S_σ is designed to make sure that the numerator in (29) becomes nonnegative. Therefore, the smoothed power spectrum is no less than the mean spectrum of the prior ensemble. We emphasize that (29) is computed component-wisely for each wave number ω . Furthermore, the mean of the prior ensemble remains the same.

After updating the ensemble, the spectrum is expected to be smoother than before, and the resulting smoothed spectrum would be more similar to the spectrum of the ensemble in a larger size. Since the data assimilation tends to be more effective when the ensemble size is larger, we expect that the updated ensemble with a smoothed spectrum has mitigated sampling errors.



(a) Mean power spectrum at $t = 3998$
without smoothing



(b) Mean power spectrum at $t = 3998$
with smoothing

Figure 2: K-S equation mean power spectrum comparison while varying the sample size: (a) smoothing is *not* applied and (b) smoothing is applied

We demonstrate this idea by testing the spectrum smoothing for the state samples of Lorenz 96 and Kuramoto-Sivashinsky models solved by the 4th-order Runge-Kutta method in Figs 1 and 2, respectively. This is a free-run simulation, i.e., assimilation using new observation does not happen. We observe that the mean power spectrum tends to be smoother as the sample size increases. Furthermore, when applying the spectrum smoothing, the mean power spectrum becomes closer to the spectrum of 1000 and 500 samples, respectively. This demonstrates that the ensemble update using the spectrum smoothing works as intended. The updated ensemble with a smoother spectrum is demonstrated to mitigate the sampling error effectively and improve the performance of ETKF accordingly, which will be presented in Section 4.

Algorithm 1 describes the ETKF with the spectrum smoothing. The *prior* ensemble $\hat{\mathbf{m}}_{j+1}$ is updated by a rescaling factor α , which mitigates the sampling errors. After the ensemble update, localization and inflation are still necessary since they alleviate other sources of errors such as model, observation characteristics, etc., as discussed in Section 2.3. Therefore, in Section 4, the performance of Algorithm 1 is tested along with the classic ETKF with localization and inflation for a fair comparison.

4 Numerical Experiments

The sampling error mitigation effect by smoothing the spectrum is demonstrated through various numerical tests in this section. Lorenz 96 model and Kuramoto-Sivashinsky (K-S) equation are some of the most commonly discussed and tested nonlinear problems in data assimilation to assess the efficacy of each scheme due to the chaotic behavior of their solutions. Moreover, the performance of classical sampling error correction techniques, including localization and inflation, and the suggested smoothing idea are compared while they are applied to ETKF. Not only measuring the prior and posterior errors, it also investigates how the ensemble updated by smoothing affects the mean

Algorithm 1 ETKF with the spectrum smoothing

Initialize the ensemble \mathbf{v}_j^k . Choose parameters c , ρ , and σ

for $j = 1$ to $J - 1$ **do**

 Compute the prior ensemble $\hat{\mathbf{v}}_{j+1}^{(k)} = \Psi(\mathbf{v}_j^{(k)})$ for $k = 1, \dots, K$.

if observations are available at $j + 1$ -th time step **then**

 Compute the prior mean $\hat{\mathbf{m}}_{j+1} = \frac{1}{K} \sum_{k=1}^K \hat{\mathbf{v}}_{j+1}^{(k)}$.

 Compute centered ensemble $\hat{X}_{j+1} = \frac{1}{\sqrt{K-1}} \left[\hat{\mathbf{v}}_{j+1}^{(1)} - \hat{\mathbf{m}}_{j+1}, \dots, \hat{\mathbf{v}}_{j+1}^{(K)} - \hat{\mathbf{m}}_{j+1} \right] =$

$\left[\hat{\mathbf{x}}_{j+1}^{(1)}, \dots, \hat{\mathbf{x}}_{j+1}^{(K)} \right]$.

 Update the prior ensemble using the spectrum smoothing for the sampling error mitigation:

$$\hat{\mathbf{v}}_{j+1}^k \leftarrow \mathcal{F}^{-1}(\mathcal{F}(\hat{\mathbf{m}}_{j+1}) + \alpha \mathcal{F}(\hat{\mathbf{x}}_{j+1}^{(k)})),$$

 where \mathcal{F} and \mathcal{F}^{-1} are discrete Fourier and inverse Fourier transforms, and α is computed as in (29).

 Inflate the prior ensemble spread: $\hat{\mathbf{v}}_{j+1}^{(k)} \leftarrow \hat{\mathbf{m}}_{j+1} + \sqrt{\rho} \hat{\mathbf{x}}_{j+1}^{(k)}$

 Update the prior covariance matrix with a localization: $\hat{C}_{j+1} \leftarrow L_c \odot \hat{C}_{j+1}$.

 Compute the Kalman gain K_{j+1} , transformation matrix T_{j+1} and X_{j+1} according to (7), (11) and (12), respectively.

 Compute the posterior ensemble and its mean as in (9) and (8).

end if

end for

spectrum and what the rescaling factor for smoothing looks like. We also discuss how spectrum smoothing changes the ETKF's sensitivity to the choice of tuning parameters of localization and inflation.

4.1 Metrics

In order to measure the prior and posterior errors, the root mean square error (RMSE) of classic ETKF and ETKF with the suggested ensemble smoothing are compared. Posterior RMSE at j th time step is defined as the following,

$$\text{RMSE}_j = \sqrt{\frac{\|\mathbf{m}_{j+1} - \mathbf{u}_{j+1}\|_2^2}{N}}, \quad (30)$$

where \mathbf{m}_{j+1} is the mean posterior ensemble, and \mathbf{u}_{j+1} is the reference solution at j th time step. For comparing the performance, the mean RMSE is computed by averaging RMSE_j over the last 350 observation time steps (i.e., analysis time step), excluding the time step where new observation is not available. We denote the observation time step size as Δt_{obs} , and then the average *posterior* RMSE is:

$$\text{RMSE} = \frac{1}{J_{obs}} \sum_{j'=1}^{J_{obs}} \text{RMSE}_{j'}, \quad (31)$$

where j' denotes the index for the observation time step. On the other hand, *prior* RMSE is computed by using the mean prior ensemble, $\hat{\mathbf{m}}_{j+1}$, instead of \mathbf{m}_{j+1} .

4.2 Lorenz 96 model

Edward Lorenz introduced the Lorenz 96 model for a better understanding of the predictability of the atmosphere, and it is still frequently used as a simplified turbulent flow model. The following system of nonlinear ODEs expresses the model: for $n = 1, \dots, N$,

$$\frac{du_n}{dt} = (u_{n+1} - u_{n-2})u_{n-1} - u_n + F \quad (32)$$

where F is a forcing constant, and it is assumed that $u_{-1} = u_{N-1}$, $u_0 = u_N$ and $u_{N+1} = u_1$ which makes the model translation-invariant. In our experiments, we obtain a reference solution $u_{t_j} \in \mathbb{R}^N$ for $j \in [J] := \{0, 1, 2, \dots, J\}$ using Lorenz 96 evolution operator, G , such that $u_{t_{j+1}} = G(u_{t_j})$, a fixed initial u_{t_0} , and a time step $\Delta t = t_{j+1} - t_j$. Lorenz 96 shows chaotic behavior when $F \geq 8$. Therefore, we obtain a reference solution of Lorenz 96 with $F = 8$. The number of variables, N , is set to 128, which is large enough to estimate the decay rate of the energy spectrum of the reference solution closely. The fourth-order Runge-Kutta method with a time step $\Delta t = 0.01$ is used to guarantee the stability while solving the given model for $t \in [0, 200]$. The initial state is set to a vector whose elements are all 8 except the first component perturbed by adding 0.01. The reference solution after the turbulence is fully developed is shown in Fig 3. For the data assimilation by ETKF, the observation time step Δt_{obs} is set to 0.15. Observations contain 10% observation noise following $\mathcal{N}(\mathbf{0}, \Gamma)$ where $\Gamma = (0.1s)^2 I_M$ and s is the standard deviation of the state solution.

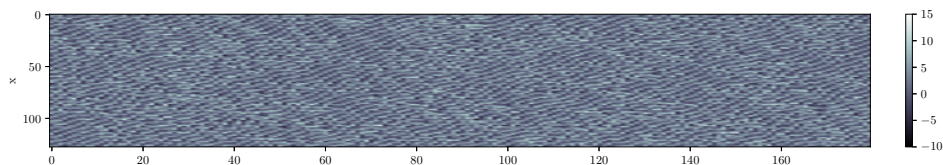


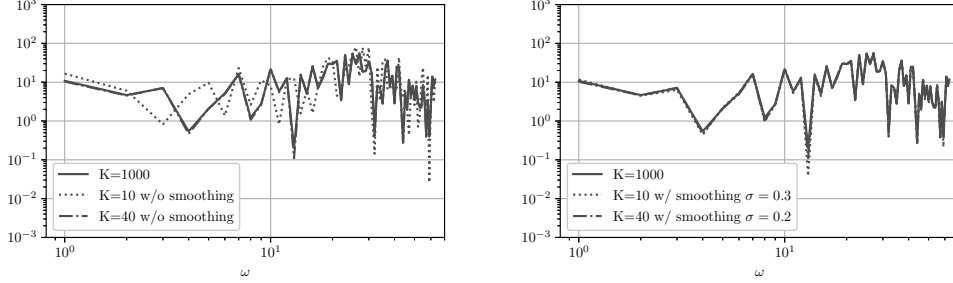
Figure 3: Lorenz 96 reference solution

4.2.1 Ensemble spectrum

Fig 4 compares the mean power spectra of *prior* ensemble of size $K = 10, 40$ and 1000 at time $t = 48.8$. We compare the classic ETKF without spectrum smoothing and our ETKF with spectrum smoothing while varying the ensemble size. It is worth noting that Fig 1 is different from Fig 4 since Fig 1 shows the mean spectrum from the free-running model without assimilation. It is observed that both ensembles of $K = 40$ with and without smoothing show power spectra similar to the spectrum of $K = 1000$. In contrast, the ensemble of $K = 10$ shows a significant difference depending on whether smoothing is applied. The ensemble of $K = 10$ updated by smoothing shows a spectrum much closer to the one from the ensemble of $K = 1000$, which is expected to be more similar to the true energy spectrum. Moreover, from Table 1 of *posterior* RMSEs, we can confirm that the ensemble of $K = 40$ with and without smoothing and the ensemble of $K = 10$ with smoothing achieve the posterior RMSE less than the baseline error. However, the ensemble

of $K = 10$ without smoothing cannot recover the Lorenz 96 solution well, even though localization and inflation are applied. Here, the baseline error is the standard deviation of measurement noise.

Fig 5 shows the rescaling factor, $\alpha(\omega)$, in the Fourier domain and its discrete inverse Fourier transform, $\mathcal{F}^{-1}(\alpha)$, in the physical domain for mitigating the sampling error. The rescaling factor $\alpha(\omega)$ is multiplied point-wisely to each discrete Fourier transform of the centered ensemble member as described in Algorithm 1. On the other hand, $\mathcal{F}^{-1}(\alpha)$ is convolved with each centered ensemble member, and therefore, it can be considered as a smoothing kernel.



(a) Mean power spectrum at $t = 48.8$, $K = 10$ (b) Mean power spectrum at $t = 48.8$, $K = 40$

Figure 4: Lorenz 96 *prior* ensemble spectrum comparison varying the ensemble size: (a) without spectrum smoothing (b) with spectrum smoothing

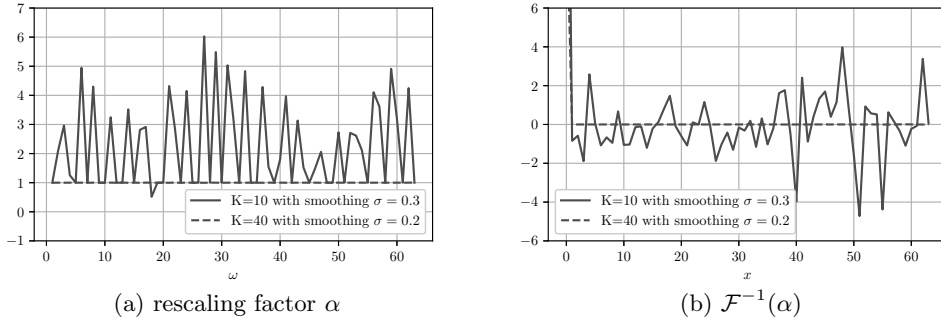


Figure 5: Lorenz 96 rescaling factor in the Fourier (left) and physical (right) domains

4.2.2 Results and sensitivity analysis

Table 1 compares the average *posterior* RMSEs of the classic ETKF and ETKF with smoothing applied to solve the Lorenz 96 model with forcing constant $F = 8$ across various ensemble sizes and observation percentages. Localization and inflation are applied to both methods, i.e., relevant parameters $c \in [1, 13]$ and $\rho \in [1.0, 1.3]$ are tuned, respectively. As $\Delta t_{obs} = 0.15$ over $t \in [0, 200]$, 1333

assimilations are performed. In Table 1, we observe that if the ensemble size and the observation percentage are large, then the two methods perform similarly as the average RMSEs of the two methods are similar, respectively. On the other hand, if either the ensemble size or observation percentage is small, then the performance of the classic ETKF degrades while ETKF with smoothing still shows RMSE lower or at least closer to baseline error. This result demonstrates that updating the ensemble through spectrum smoothing based on the smooth constraint of the energy spectrum mitigates the sampling error successfully.

Figs 7 and 8 show the time series of *prior* and *posterior* errors, respectively. In addition to the average error, the error time series also confirms that ETKF with smoothing helps mitigate the sampling errors, and eventually, the error time series gets smaller as ETKF proceeds, regardless of the ensemble size and observation percentages. Moreover, Fig 9 shows the pointwise error of the *prior* and *posterior* solutions compared to the reference solution in Fig 3. ETKF with smoothing shows prior and posterior solutions close to the reference once the assimilation is stabilized, while the solutions from the classic ETKF show clearly different patterns over the entire time when the ensemble size is as small as 10, or the observation percentage is as small as 25%. Additionally, in Fig 6, we can confirm that spectrum smoothing makes ETKF consistently work well across the various choices of c and ρ . It implies that smoothing helps to reduce the sensitivity to the tuning parameters of localization and inflation. Localization and inflation are essential tools to make the data assimilation work stably when the sampling error is large, but fine-tuning is necessary depending on the ensemble size and observation percentage. In Fig 6, the classic ETKF works well only for limited choices of c and ρ , while the ETKF with smoothing shows excellent performance across a wide range of parameters.

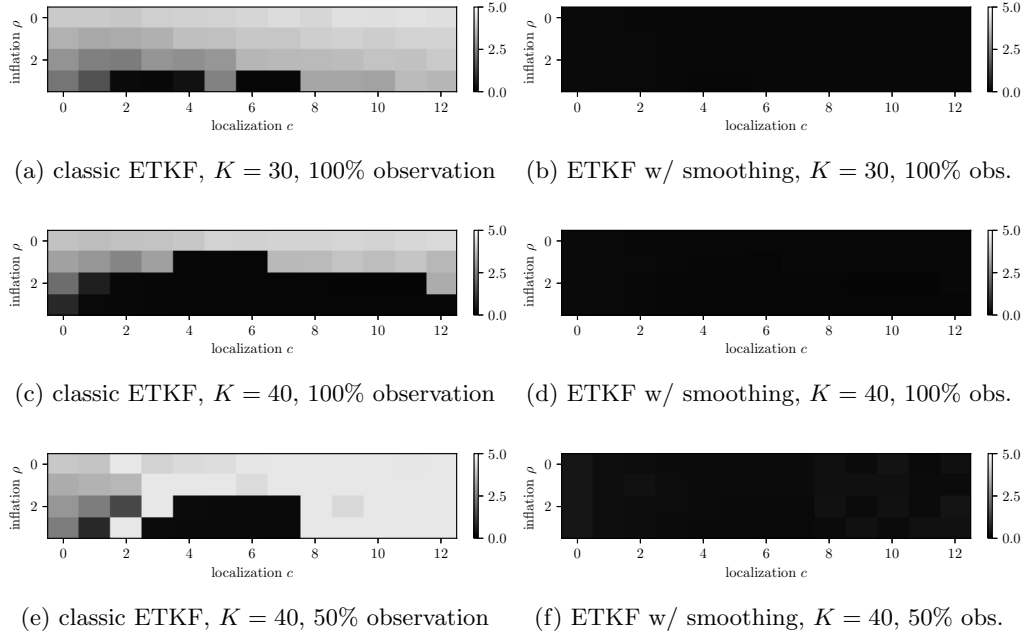
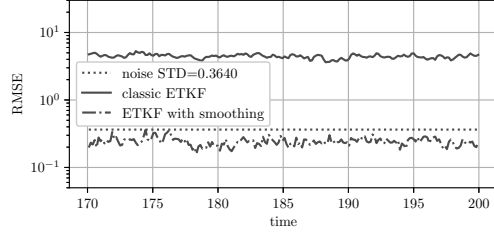


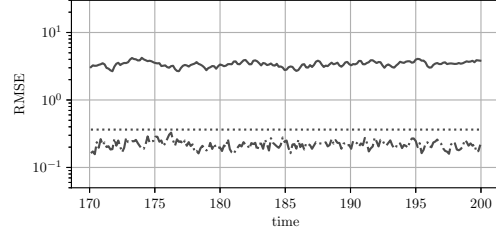
Figure 6: *Posterior* RMSE sensitivity to localization and inflation

	K	Observation	c	ρ	σ	RMSE
classic ETKF	10	100%	1	1.3		4.1707
ETKF w/ smoothing	10	100%	5	1.2	0.3	0.1833
classic ETKF	10	50%	1	1.3		4.334
ETKF w/ smoothing	10	50%	2	1.0	0.4	0.3862
classic ETKF	10	33%	1	1.3		4.4867
ETKF w/ smoothing	10	33%	2	1.0	0.4	1.3019
classic ETKF	10	25%	1	1.3		4.4515
ETKF w/ smoothing	10	25%	1	1.2	0.4	3.2312
classic ETKF	20	100%	2	1.3		3.242
ETKF w/ smoothing	20	100%	8	1.1	0.3	0.1635
classic ETKF	20	50%	1	1.3		3.6481
ETKF w/ smoothing	20	50%	8	1.2	0.3	0.2346
classic ETKF	20	33%	1	1.3		4.0481
ETKF w/ smoothing	20	33%	8	1.3	0.3	0.3054
classic ETKF	20	25%	1	1.3		3.9243
ETKF w/ smoothing	20	25%	3	1.1	0.4	2.5795
classic ETKF	30	100%	2	1.3		3.242
ETKF w/ smoothing	30	100%	8	1.1	0.3	0.1635
classic ETKF	30	50%	1	1.3		3.11
ETKF w/ smoothing	30	50%	10	1.0	0.3	0.2167
classic ETKF	30	33%	1	1.3		3.5618
ETKF w/ smoothing	30	33%	10	1.2	0.3	0.2728
classic ETKF	30	25%	1	1.3		3.7361
ETKF w/ smoothing	30	25%	4	1.1	0.4	0.8525
classic ETKF	40	100%	11	1.2		0.1143
ETKF w/ smoothing	40	100%	12	1.2	0.2	0.1134
classic ETKF	40	50%	8	1.2		0.1899
ETKF w/ smoothing	40	50%	8	1.2	0.2	0.1873
classic ETKF	40	33%	2	1.3		2.6587
ETKF w/ smoothing	40	33%	10	1.0	0.3	0.2681
classic ETKF	40	25%	1	1.3		3.4927
ETKF w/ smoothing	40	25%	7	1.2	0.4	0.5102

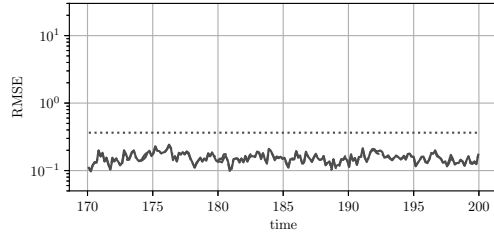
Table 1: Average *posterior* RMSE of ETKF on Lorenz 96 model with localization and inflation, $F=8$, $N = 128$, $t \in [0, 200]$, $\Delta t_{obs} = 0.15$ (1333 assimilations), baseline = 0.3640, localization parameter $c \in [1, 13]$ increasing by 1, inflation $\rho \in [1.0, 1.3]$ increasing by 0.1



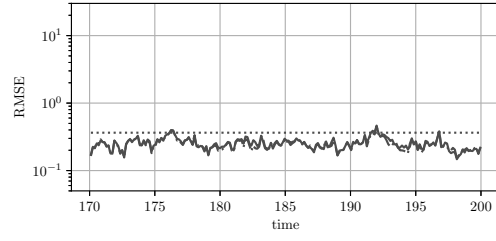
(a) $K = 10$, 100% observation



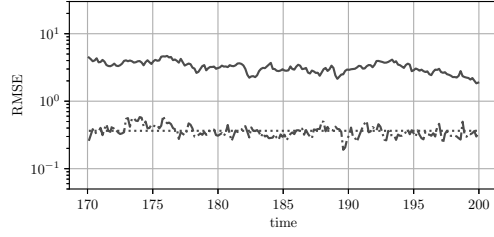
(b) $K = 20$, 100% observation



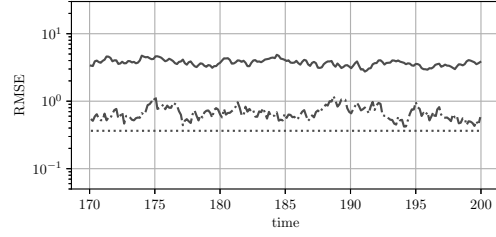
(c) $K = 40$, 100% observation



(d) $K = 40$, 50% observation

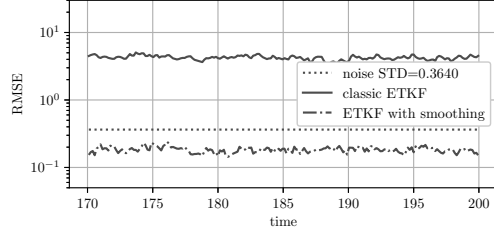


(e) $K = 40$, 33% observation

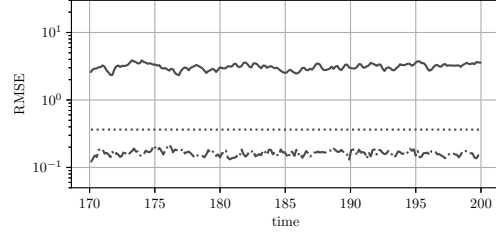


(f) $K = 40$, 25% observation

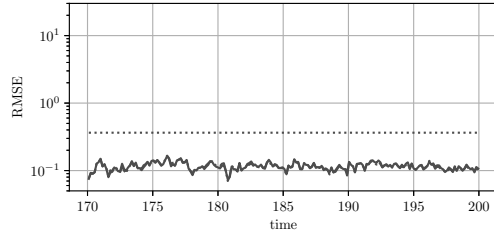
Figure 7: Lorenz 96, time series of *prior* RMSE



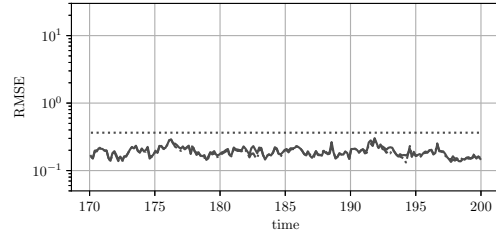
(a) $K = 10$, 100% observation



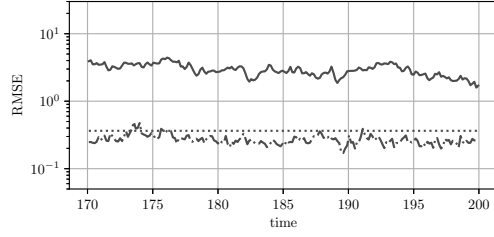
(b) $K = 20$, 100% observation



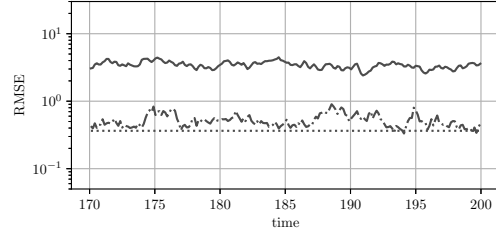
(c) $K = 40$, 100% observation



(d) $K = 40$, 50% observation



(e) $K = 40$, 33% observation



(f) $K = 40$, 25% observation

Figure 8: Lorenz 96, time series of *posterior* RMSE

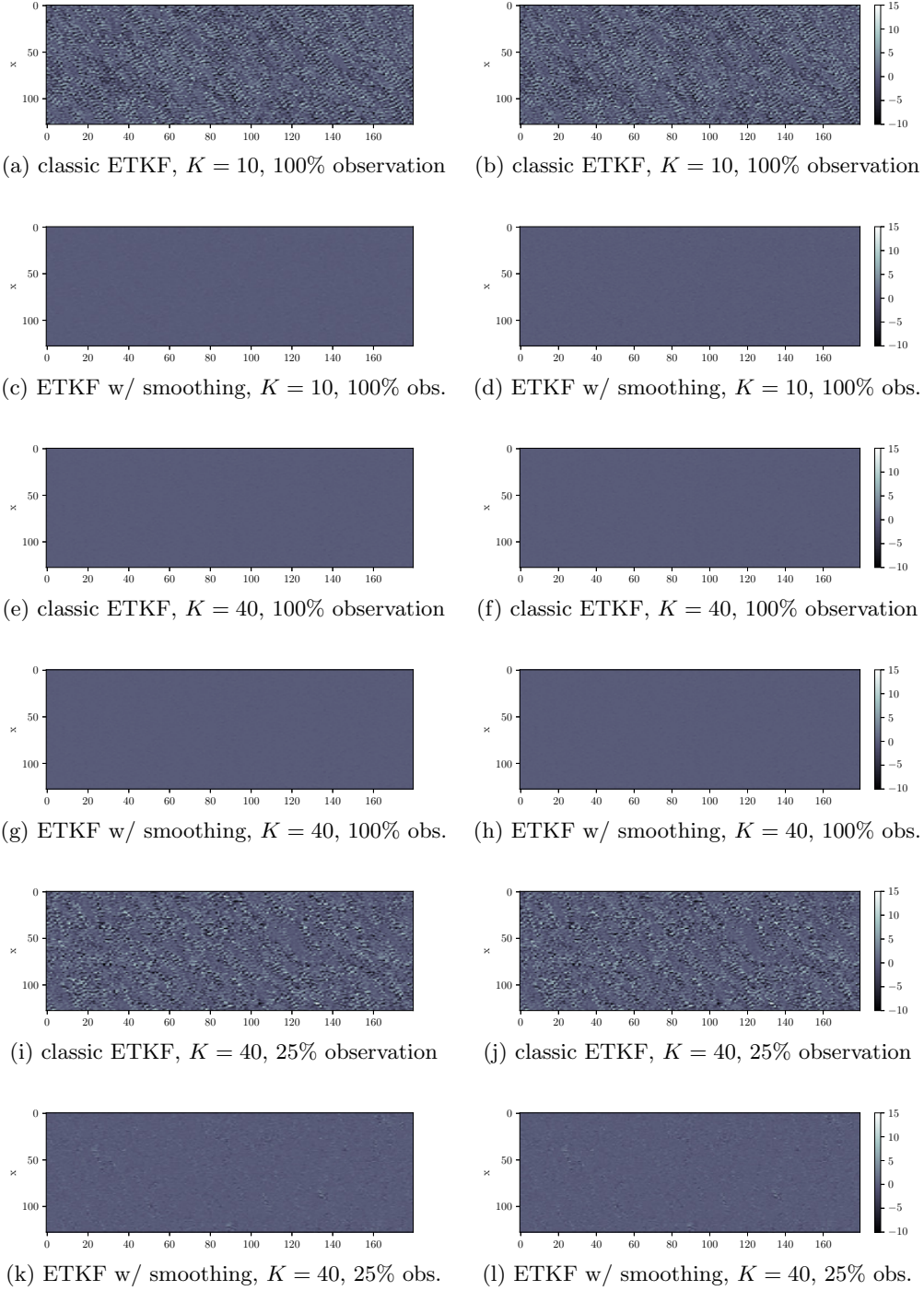


Figure 9: Pointwise difference of *prior* (left column) and *posterior* (right column) solutions from the Lorenz 96 reference solution in Fig 3

4.3 Kuramoto-Sivashinsky equation

Kuramoto-Sivashinsky (K-S) equation is a fourth-order partial differential equation which was introduced as a one-dimensional model of instability of flames and phase turbulence in chemical reactions. The equation is given as follows:

$$\begin{aligned} u_t + u_{xxxx} + u_{xx} + uu_x &= 0, \quad (x, t) \in \mathbb{R} \times \mathbb{R}^+, \\ u(x, 0) &= u_0(x), \quad x \in \mathbb{R}, \end{aligned} \quad (33)$$

where u_0 is an initial condition. K-S equation shares some features with the Navier-Stokes equation: the terms u_{xx} and u_{xxxx} in (33) below provide 1D analogs to the energy production and dissipation terms in Navier-Stokes [10]. Time-asymmetric stripe-like patterns, called “solitons”, appear and merge in its solution as in Fig 10.

In our experiments, we set u_0 as the following:

$$u_0(x) = \cos\left(\frac{x}{\nu}\right) \left(1 + \sin\left(\frac{x}{\nu}\right)\right). \quad (34)$$

Due to the periodicity of the initials, the spatial domain can be restricted to $[0, 2\nu\pi]$, and a Fourier spectral method can be used for spatial discretization. We obtain a reference solution $u_j \in \mathbb{R}^N$ for $j \in [J] := \{0, 1, 2, \dots, J\}$ with a fixed initial u_0 , and a time step $\Delta t = 0.25$. We obtain a reference solution with $\nu = 16$ in Fig 10 using the Fourier spectral method in space and ETDRK4 in time. The number of variables, N , is set to 256, and we solve the given equation for $t \in [0, 10000]$. For the data assimilation, we use the reference solution over $t \in [2000, 10000]$ where the turbulence is fully developed, and the observation time step Δt_{obs} is set to 10. Observation noise follows $\mathcal{N}(\mathbf{0}, \Gamma)$ where $\Gamma = (0.1s)^2 I_M$, and s is the solution state’s standard deviation.

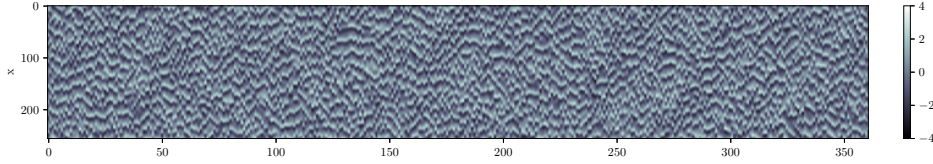
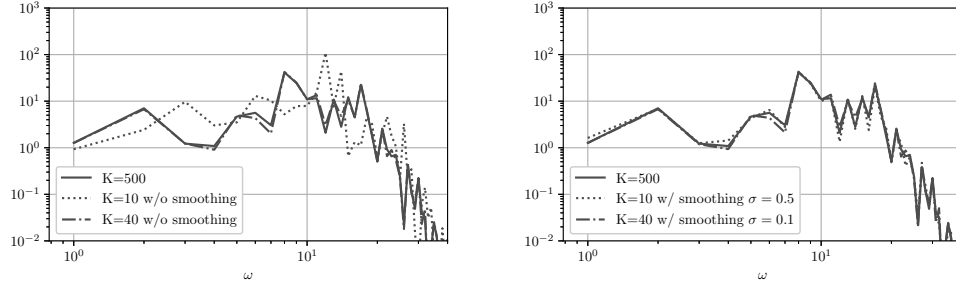


Figure 10: K-S equation reference solution

4.3.1 Energy spectrum and results

In Fig 11, mean power spectra from the ensemble of size $K = 10, 40$ and 500 are compared. We remind readers that Fig 11 shows the mean spectra when the ensemble is updated using new observations in ETKF while Fig 2 shows the spectra from the free run. Both ensembles of $K = 40$ with and without smoothing show the mean power spectra close to the one from the ensemble of $K = 500$. However, we observe that the ensemble of $K = 10$ with smoothing shows a much closer spectrum than the ensemble of $K = 10$ without smoothing. Thereby, the smoothing technique effectively mitigates the sampling error, especially when the ensemble size is small. In addition, Table 2 also shows that smoothing helps to improve the performance of ETKF regardless of the ensemble numbers and observation percentages. However, the classic ETKF cannot recover the solution of



(a) Mean power spectrum at $t = 3998$, $K = 10$ (b) Mean power spectrum at $t = 3998$, $K = 40$

Figure 11: K-S equation *prior* ensemble spectrum comparison varying the ensemble size: (a) without spectrum smoothing (b) with spectrum smoothing

the K-S equation well if either the ensemble number or observation percentage is significantly low. These results are consistent with the ones from Table 1 for Lorenz 96.

Figs 12 and 13 show the time series of *prior* and *posterior* RMSE, and we observe that both classic ETKF and ETKF with smoothing show similarly low RMSE if $K = 40$ and observation is full or moderately sparse as 33% or 50%. However, when the observation percentage drops to 25%, or the ensemble number drops to as low as 10, then ETKF with smoothing shows RMSE much less than the baseline over time, while the classic ETKF fails to achieve RMSE close to the baseline. In addition, Figs 9 and 14 show the pointwise errors of *prior* and *posterior* solutions from the reference in Fig 10, respectively. It demonstrates that ETKF with smoothing over the spatio-temporal domain recovers most of solitons accurately whether the ensemble number or observation percentage is large or not. On the other hand, inaccurate solitons are observed in the classic ETKF's solutions leading to large pointwise errors if ensemble number is as small as 10 or observation is very sparse as 25%.

5 Discussions and conclusions

Ensemble Kalman Filter's performance is highly dependent on the ensemble size as the small number of samples increases the sampling error. Large ensemble size is required for stable performance, but computational cost to solve the problems for the prediction often prevents to increase the ensemble number as desired. Due to this reason, our work suggests updating the ensemble without increasing their number based on the solution's characteristics: smooth constraint in its energy spectrum. Numerical tests in various settings with Lorenz 96 model and Kuramoto-Sivashinsky equation demonstrate that smoothing technique significantly improves the performance of ETKF with localization and inflation even for the very small ensemble size where the classic ETKF cannot recover the solutions well. Moreover, the classic ETKF has difficulty in recovering the solutions from very sparse observation which is also possible to increase the sampling error. Smoothing technique shows its consistently stable performance for sparse observation. Even though both ETKF with and without smoothing require localization and inflation, sensitivity analysis with Lorenz 96 shows that smoothing makes ETKF less sensitive to the tuning parameters for localization and inflation.

In this work, ETKF with smoothing shows different performances depending on the choice of smoothing kernel width. Even though their performances are less sensitive than the localization and inflation parameters, we will investigate how to choose the optimal kernel width depending on problems in future work. Moreover, the Gaussian kernel is used in this work, but designing optimal kernels will be another interesting work in the future. The k-S equation requires a larger smoothing kernel width than Lorenz 96, so we guess that the spectrum decay rate is relevant to the smoothing kernel width. Also, ensemble size and observation percentage may affect its choice. On the other hand, we use the smoothing characteristics of the energy spectrum, which gives global information on solutions to update the ensemble and mitigate the sampling errors. However, there can be other quantities that have smooth characteristics, such that the larger ensemble size shows smoother quantities than the smaller ensemble size. We will investigate such other characteristics in future work. Another future work is to analyze how the smoothing technique rigorously reduces the sampling error. It will be helpful to investigate how smoothing affects the Lyapunov space.

Prior information about dynamical solutions can be integrated as covariance in various forms other than smooth constraints. In [15], the second moment of the gradient information is used to design a covariance matrix for applying ETKF to dynamical systems with discontinuous solution profiles. In this work, a weighting matrix is introduced for enforcing the recovery of sparse solutions while maintaining the form of ℓ_2 regularized optimization. However, it has been well-studied that ℓ_1 regularization effectively recovers sparse solutions. On the other hand, if solutions have multiple features, including discontinuities and oscillations, inhomogeneous regularization effectively recovers disparate features [9, 4] for static image recovery. Designing inhomogeneous regularizations dynamically in the context of data assimilation has yet to be studied, which will be another interesting future work.

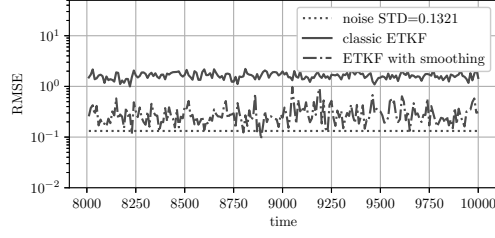
Acknowledgement

Yoonsang Lee is supported by ONR MURI N00014-20-1-2595.

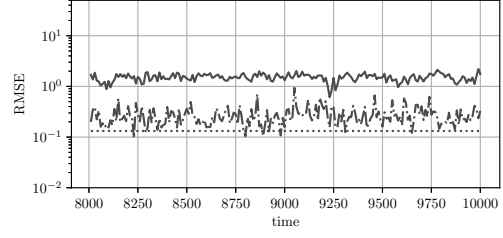
References

- [1] J. L. Anderson. An adaptive covariance inflation error correction algorithm for ensemble filters. *Tellus A: Dynamic Meteorology and Oceanography*, 59(2):210–224, 2007.
- [2] J. L. Anderson. Localization and sampling error correction in ensemble kalman filter data assimilation. *Monthly Weather Review*, 140(7):2359 – 2371, 2012.
- [3] C. Chatfield. *The analysis of time series: an introduction*. CRC Press, Florida, US, 6th edition, 2004.
- [4] B. Choi, J. Han, and Y. Lee. Weighted inhomogeneous regularization for inverse problems with indirect and incomplete measurement data, 2024.
- [5] A. J. Chorin. *Vorticity and turbulence*, volume 103. Springer Science & Business Media, 2013.
- [6] G. Evensen. Sequential data assimilation with a nonlinear quasi-geostrophic model using monte carlo methods to forecast error statistics. *Journal of Geophysical Research: Oceans*, 99(C5):10143–10162, 1994.

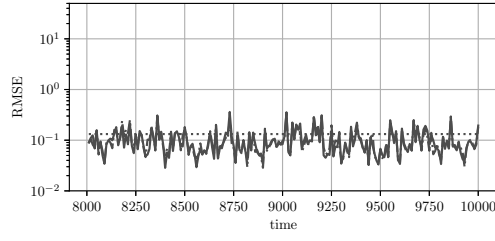
- [7] N. J. Gordon, D. J. Salmond, and A. F. Smith. Novel approach to nonlinear/non-gaussian bayesian state estimation. In *IEE proceedings F (radar and signal processing)*, volume 140, pages 107–113. IET, 1993.
- [8] T. M. Hamill, J. S. Whitaker, and C. Snyder. Distance-dependent filtering of background error covariance estimates in an ensemble kalman filter. *Monthly Weather Review*, 129(11):2776–2790, 2001.
- [9] J. Han and Y. Lee. Inhomogeneous regularization with limited and indirect data. *Journal of Computational and Applied Mathematics*, 428:115193, 2023.
- [10] P. Holmes, J. L. Lumley, G. Berkooz, and C. W. Rowley. *Turbulence, Coherent Structures, Dynamical Systems and Symmetry*. Cambridge Monographs on Mechanics. Cambridge University Press, 2 edition, 2012.
- [11] A. Jazwinski. *Stochastic Processes and Filtering Theory*. Mathematics in Science and Engineering. Elsevier Science, 1970.
- [12] R. E. Kalman. A New Approach to Linear Filtering and Prediction Problems. *Journal of Basic Engineering*, 82(1):35–45, 03 1960.
- [13] E. Kalnay. *Atmospheric Modeling, Data Assimilation and Predictability*. Cambridge University Press, 2002.
- [14] K. Law, A. Stuart, and K. Zygalakis. *Data assimilation: A mathematical introduction*, volume 62 of *Texts in Applied Mathematics*. Springer, Cham, 2015. A mathematical introduction.
- [15] T. Li, A. Gelb, and Y. Lee. A structurally informed data assimilation approach for nonlinear partial differential equations, 2024.
- [16] R. Rood, G. Gaspari, and S. Cohn. Construction of correlation functions in two and three dimensions. *Quarterly Journal of the Royal Meteorological Society*, 125, 05 1998.
- [17] A. Spantini, R. Baptista, and Y. Marzouk. Coupling techniques for nonlinear ensemble filtering. *SIAM Review*, 64(4):921–953, 2022.
- [18] M. K. Tippett, J. L. Anderson, C. H. Bishop, T. M. Hamill, and J. S. Whitaker. Ensemble square root filters. *Monthly Weather Review*, 131(7):1485 – 1490, 2003.
- [19] X. Wang and C. H. Bishop. A comparison of breeding and ensemble transform kalman filter ensemble forecast schemes. *Journal of the atmospheric sciences*, 60(9):1140–1158, 2003.
- [20] Z. Wang, L. Lei, J. Anderson, Z.-M. Tan, and Y. Zhang. Convolutional neural network-based adaptive localization for an ensemble kalman filter. *Journal of Advances in Modeling Earth Systems*, 15, 10 2023.



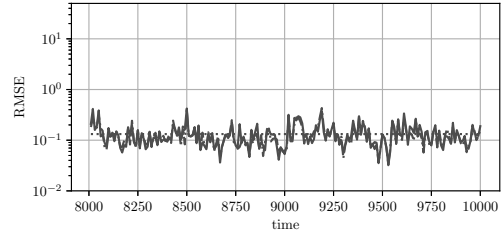
(a) $K = 10$, 100% observation



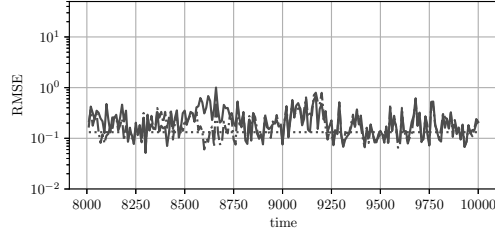
(b) $K = 20$, 100% observation



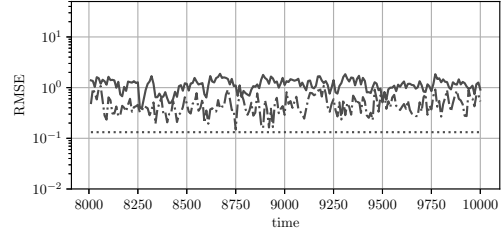
(c) $K = 40$, 100% observation



(d) $K = 40$, 50% observation

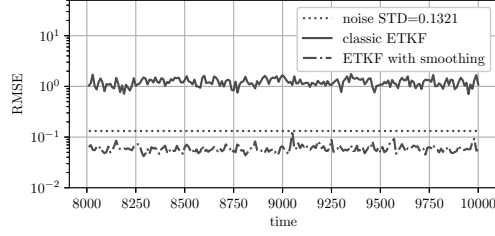


(e) $K = 40$, 33% observation

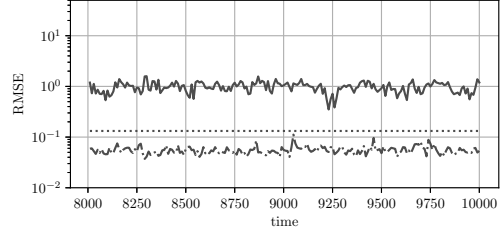


(f) $K = 40$, 25% observation

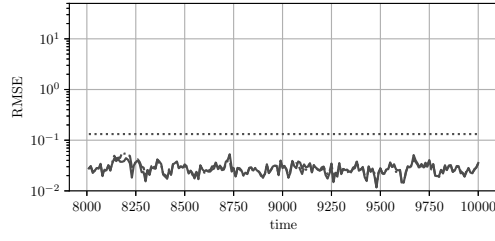
Figure 12: K-S equation, time series of *prior* RMSE



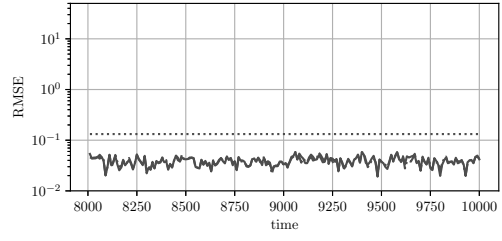
(a) $K = 10$, 100% observation



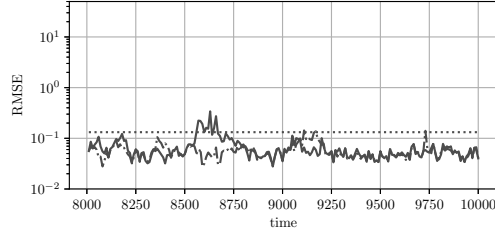
(b) $K = 20$, 100% observation



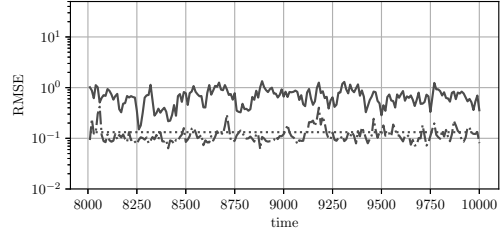
(c) $K = 40$, 100% observation



(d) $K = 40$, 50% observation



(e) $K = 40$, 33% observation



(f) $K = 40$, 25% observation

Figure 13: K-S equation, time series of *posterior* RMSE

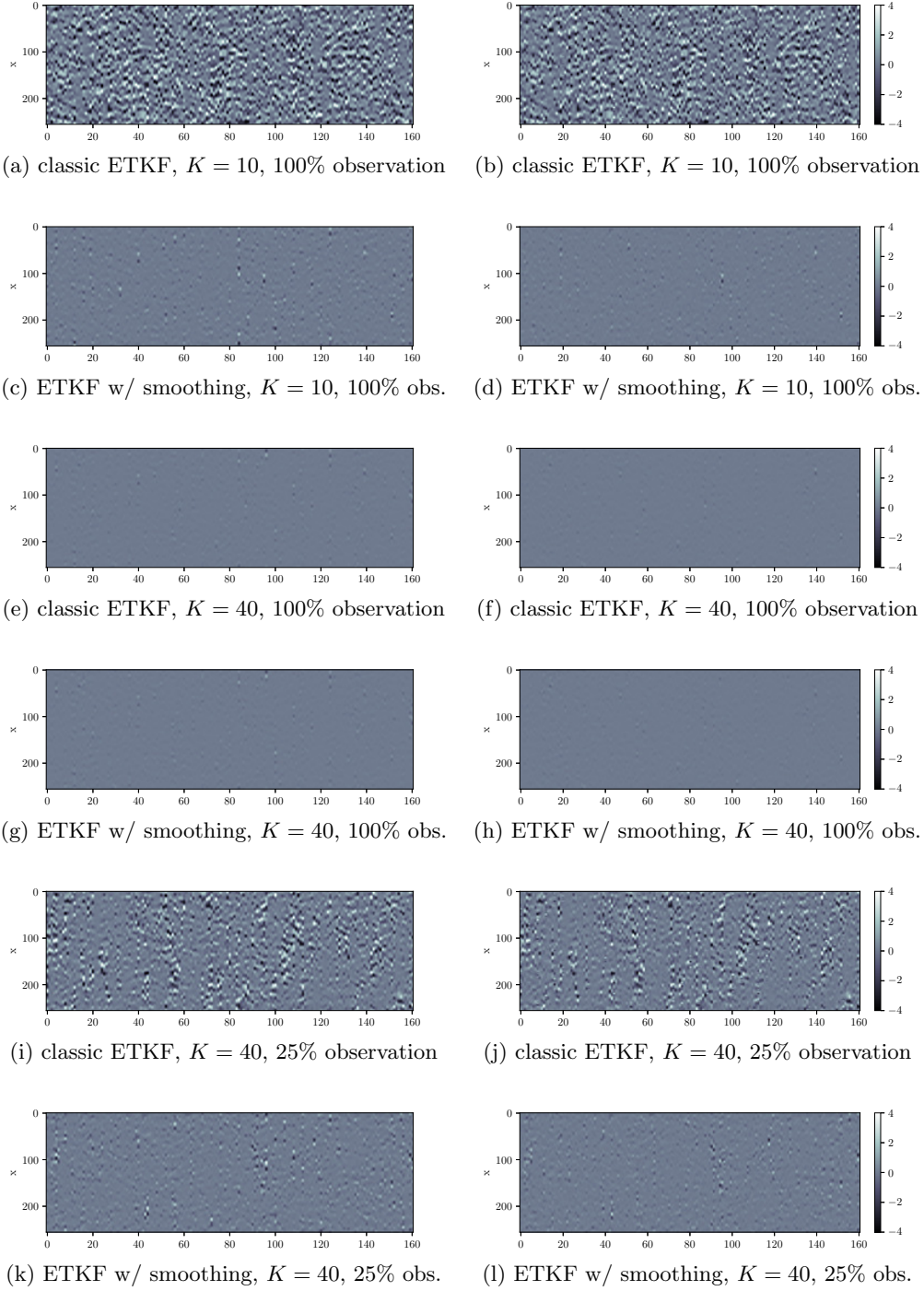


Figure 14: Pointwise difference of *prior* (left column) and *posterior* (right column) solutions from the K-S equation's reference solution in Fig 10

	K	Observation	c	ρ	σ	RMSE
classic ETKF	10	100%	4	1.3		1.2054
ETKF w/ smoothing	10	100%	20	1.0	0.5	0.0606
classic ETKF	10	50%	4	1.2		1.1885
ETKF w/ smoothing	10	50%	20	1.0	0.9	0.0856
classic ETKF	10	33%	6	1.3		1.2233
ETKF w/ smoothing	10	33%	20	1.1	1	0.1051
classic ETKF	10	25%	4	1.3		1.1842
ETKF w/ smoothing	10	25%	20	1.3	1	0.1218
classic ETKF	20	100%	6	1.3		0.9403
ETKF w/ smoothing	20	100%	28	1.3	0.4	0.0557
classic ETKF	20	50%	4	1.3		0.8413
ETKF w/ smoothing	20	50%	20	1.3	0.4	0.0791
classic ETKF	20	33%	4	1.3		0.876
ETKF w/ smoothing	20	33%	18	1.3	0.4	0.0983
classic ETKF	20	25%	6	1.2		0.9132
ETKF w/ smoothing	20	25%	20	1.3	0.5	0.1122
classic ETKF	30	100%	90	1.3		0.0273
ETKF w/ smoothing	30	100%	90	1.3	0.1	0.0289
classic ETKF	30	50%	98	1.2		0.0401
ETKF w/ smoothing	30	50%	90	1.3	0.2	0.0394
classic ETKF	30	33%	92	1.3		1.3673
ETKF w/ smoothing	30	33%	82	1.3	0.8	0.1001
classic ETKF	30	25%	84	1.3		1.321
ETKF w/ smoothing	30	25%	82	1.3	0.6	0.11
classic ETKF	40	100%	96	1.3		0.0271
ETKF w/ smoothing	40	100%	96	1.3	0.1	0.0275
classic ETKF	40	50%	100	1.3		0.0398
ETKF w/ smoothing	40	50%	100	1.3	0.1	0.0389
classic ETKF	40	33%	94	1.3		0.0594
ETKF w/ smoothing	40	33%	98	1.3	0.2	0.0553
classic ETKF	40	25%	6	1.2		0.6721
ETKF w/ smoothing	40	25%	6	1.2	0.5	0.1374

Table 2: Average *posterior* RMSE of ETKF on K-S equation with localization and inflation, $\nu=16$, $N = 256$, $t \in [2000, 10000]$, $\Delta t_{obs} = 10$ (800 assimilations), baseline = 0.1321, localization parameter $c \in [2, 100]$ increasing by 2, inflation $\rho \in [1.0, 1.3]$ increasing by 0.1